Primary: S5
Secondary: S2
Biochem. J. (2013) **454**, 427–435 (Printed in Great Britain) doi:10.1042/BJ20121693

online data

Zinc co-ordination by the DHHC cysteine-rich domain of the palmitoyltransferase Swf1

Ayelén GONZÁLEZ MONTORO*, Rodrigo QUIROGA* and Javier VALDEZ TAUBAS*[1]

*Centro de Investigaciones en Química Biológica de Córdoba, CIQUIBIC (UNC-CONICET), Departamento de Química Biológica, Facultad de Ciencias Químicas, Universidad Nacional de Córdoba, Ciudad Universitaria, X5000HUA Córdoba, Argentina

S-acylation, commonly known as palmitoylation, is a widespread post-translational modification of proteins that consists of the thioesterification of one or more cysteine residues with fatty acids. This modification is catalysed by a family of PATs (palmitoyltransferases), characterized by the presence of a 50-residue long DHHC-CRD (Asp-His-His-Cys cysteine-rich domain). To gain knowledge on the structure–function relationships of these proteins, we carried out a random-mutagenesis assay designed to uncover essential amino acids in Swf1, the yeast PAT responsible for the palmitoylation of SNARE (soluble *N*-ethylmaleimide-sensitive fusion protein-attachment protein receptor) proteins. We identified 21 novel loss-of-function mutations, which are mostly localized within the DHHC-CRD. Modelling of the tertiary structure of the Swf1 DHHC domain suggests that it could fold as a zinc-finger domain, co-ordinating two zinc atoms in a CCHC arrangement. All residues predicted to be involved in the co-ordination of zinc were found to be essential for Swf1 function in the screen. Moreover, these mutations result in unstable proteins, in agreement with a structural role for these zinc fingers. The conservation of amino acids predicted to form each zinc-binding pocket suggests a shared function, as the selective pressure to maintain them is lost upon mutation of one of them. A Swf1 orthologue that lacks one of the zinc-binding pockets is able to complement a yeast *swf1Δ* strain, possibly because a similar fold can be stabilized by hydrogen bonds instead of zinc co-ordination. Finally, we show directly that recombinant Swf1 DHHC-CRD is able to bind zinc. Sequence analyses of DHHC domains allowed us to present models of the zinc-binding properties for all PATs.

Key words: DHHC domain, palmitoyltransferase, yeast, Swf1, zinc finger.

INTRODUCTION

Palmitoylation or S-acylation is a widespread post-translational modification of proteins. It involves the addition of a long-chain fatty acid to a cysteine residue through thioestherification. This modification is the only lipid modification that is reversible and therefore capable of regulatory activities [1–3]. Palmitoylation is involved in important biological processes such as the visual cycle, synaptic transmission and signal transduction [4–7]. These roles are carried out by controlling the function, localization and stability of numerous proteins (reviewed in [8,9]). New interesting roles for palmitoylation continue to emerge [10,11].

S-acylation is mediated by a family of polytopic membrane proteins containing four to six TMDs (transmembrane domains). This family is characterized by the presence of a 50-residue-long conserved domain called the DHHC-CRD (Asp-His-His-Cys cysteine-rich domain).

Within the domain there is a DHHC motif which is almost invariant across the whole family. Outside this domain, two other short motifs, TTxE (where x is any amino acid) and DPG are highly conserved. Finally, the PaCCT [PAT (palmitoyltransferase) conserved C-terminus] motif is present in most PATs [12]. Intriguingly, the remaining protein regions display little sequence conservation across the family, even when comparing orthologues from closely related organisms [13,14].

Despite the importance of PATs, there is little information regarding the structure–function relationships in these proteins. Mutations in the DHHC domain have been obtained for a few PATs; in particular, mutation of the cysteine residue in the DHHC motif resulted in loss of PAT activity for all PATs analysed, which led us to hypothesize that this motif is crucial for catalysis [15–17]. Additionally, several conserved residues within the DHHC-CRD have been mutated for the yeast PATs Erf2 and Pfa3, the PATs responsible for the palmitoylation of Ras2 and Vac8 respectively, resulting in lack of function in most but not all cases [18,19].

Besides being responsible for catalysis, the DHHC-CRD might have additional functions. We have recently shown that DHHC-CRDs are not interchangeable among different PATs and proposed, on the basis of bioinformatic and mutagenic analyses, that these domains might also be involved in the determination of enzyme specificity [13].

Outside the DHHC-CRD, Tyr^{323} within the PaCCT motif has been shown to be essential for Swf1 function [12]. Also within the C-terminal domain, Phe^{233} has been shown to be essential for DHHC21 function and localization. Mice bearing a deletion of this amino acid present the 'depilated' phenotype, characterized by variable hair loss, with thinner and shorter hairs remaining in a greasy coat [20].

Regarding the mechanism of protein palmitoylation, the involvement of a covalent PAT–palmitate intermediate had been postulated based on the fact that several PATs were shown to autoacylate. Recently, using yeast Erf2 as a model, it was shown that the palmitoylation reaction occurs in two steps, a first one involving the formation of a palmitoyl–Erf2

Abbreviations used: SC – URA, synthetic complete lacking uracil; CRD, cysteine-rich domain; ERAD, endoplasmic reticulum-associated degradation; ICP-MS, inductively coupled plasma MS; ML, maximum likelihood; ORF, open reading frame; PaCCT, palmitoyltransferase conserved C-terminus; PAT, palmitoyltransferase; biotin–BMCC, 1-biotinamido-4-[4-maleimidomethyl)-cyclohexane-carboxamido]butane; SNARE, soluble *N*-ethylmaleimide-sensitive fusion protein-attachment protein receptor; TMD, transmembrane domain; wt, wild-type.

[1] To whom correspondence should be addressed (email jvaldezt@dqb.fcq.unc.edu.ar).

© The Authors Journal compilation © 2013 Biochemical Society

intermediate followed by the transfer of the palmitoyl moiety to the substrate protein [21]. For mammalian DHHC2 and DHHC3, a single turnover assay showed that radiolabelled acyl groups are transferred from the PAT to the substrate, confirming a Ping Pong mechanism for these enzymes [22].

In order to increase our knowledge of PAT structure and function, we carried out a screen to isolate lack-of-function mutations in a representative member of the family, the PAT Swf1. Swf1 is responsible for the S-acylation of single-spanning membrane proteins such as transmembrane SNAREs (soluble *N*-ethylmaleimide-sensitive fusion protein-attachment protein receptor) [19] and glycosyltransferases [17]. In both cases, target cysteine residues are located at the cytosolic border of their TMDs. Unlike other PATs, which seem to have overlapping specificities, Swf1 is highly specific for its substrates [13], making it an interesting model protein for structure–function analyses. Moreover, a *swf1Δ* strain has some easy-to-assess phenotypes, which provide a convenient way to isolate and test Swf1 mutations.

In the present study, we begin the characterization of over 20 novel Swf1 loss-of-function mutations, which are mostly localized within the DHHC-CRD. The DHHC-CRD of PATs was initially described as having homology with a Cys_4 zinc finger followed by a complex cysteine/histidine-rich region [23] and also as a non-Cys_2His_2 zinc finger named NEW1 [24]. However, there is no structural information available and the binding of zinc by DHHC proteins has not been demonstrated [14]. It has been postulated that the zinc-binding domain would not be required for general palmitoylation activity, since PATs such as Pfa5, Akr2 and Akr1 do not seem to have a CRD and hence would not bind zinc [14]. In the present study we address the issue of zinc co-ordination by the DHHC-CRD of Swf1 and suggest models of zinc co-ordination for the whole family of PATs.

EXPERIMENTAL

Plasmids and strains

The strains used in the present study are BY4742 from the EUROSCARF consortium, or derivatives containing complete deletions of SWF1 or UBC7 ORFs (open reading frames). The plasmid for bacterial expression of Swf1 DHHC-CRD (pJV 501) is a pGEX-4T3 (GE Healthcare Life Sciences) that encodes the cytosolic loop between Swf1 TMDs 2 and 3, from Met^{103} to Gln^{178} (see Supplementary Figure S1 at http://www.biochemj.org/bj/454/bj4540427add.htm). The band was amplified by PCR using the oligonucleotides Swf1 40 (5′-AAACTCGAGATGGTAAGCAGAGCTGAGG-3′) and 41 (5′-TTTAAGCTTCATTGAAGGTAGTTTCCCTTTCC-3′). Plasmids for expression of the mutated Swf1-DHHC-CRDs were obtained likewise using the mutated plasmids obtained in the screen as templates for the corresponding PCRs.

Yarrowia lipolytica SWF1 ORF YALI0B01606g was amplified from *Y. lipolytica α121-1B* genomic DNA using the oligonucleotides YARLI-SWF1 01 (5′-AAAGGATCCATGTGGCTCAAAATCTACC-3′) and 02 (5′-TTTGTCGACCTAATAAGCGCTGTTCGG-3′), digested with BamHI/SalI and cloned in the same sites in pJV29, a YCplac33-based plasmid containing the TPI1 promoter and the PGK1 terminator.

Isolation of Swf1 mutants by error-prone PCR

A YCplac33-based plasmid containing the TPI1 promoter and the PGK1 terminator was removed of its EcoRI site by filling the overhangs with the Klenow fragment DNA polymerase (Promega) generating 29ΔEcoRI. The Swf1 coding sequence was obtained by digestion with BamHI /SalI from pJV322 [13] and cloned in the same sites in 29ΔEcoRI generating 29ΔEcoRI-Swf1.

29ΔEcoRI-Swf1 was used as a template for error-prone PCR, using oligonucleotides M13-F and M13-R generating a PCR fragment which includes sequences 459 bp upstream of SWF1 ATG and 320 bp downstream of the stop codon, for efficient gap repair. The PCR conditions were: 14 μM $MgCl_2$, 0.114 μM $MnCl_2$, 5 units of Taq polymerase (Invitrogen), 0.2 mM dATP, 0.2 mM dGTP, 1 mM dCTP and 1 mM dTTP to enhance the mutation rate. A 100 μl PCR was carried out in ten aliquots of 10 μl, to avoid over-representation of mutations produced in early PCR cycles.

The 29ΔEcoRI plasmid was digested with BamHI/SalI and co-transformed into *Δswf1* yeast with the PCR product, in a 1:1 molar ratio, adding up to 1 μg of DNA. A total of 30000 colonies were plated in SC − URA (synthetic complete lacking uracil) medium, grown to an average diameter of 1 mm and replicated to YP lactate [1 % (w/v) yeast extract/2 % (w/v) peptone] plates that contained 2 % sodium (DL)-lactate (Sigma) as the sole carbon source, using sterile velvet. The YP lactate plates were incubated at 30 °C overnight and colonies that did not grow were streaked from the original SC − URA plate to fresh plates. The phenotypes of the selected clones were confirmed by growth tests on solid medium, plated with serial dilutions of an overnight culture. The strains that presented diminished growth in both YP lactate and YPD [1 % (w/v) yeast extract/2 % (w/v) peptone/2 % (w/v) glucose] plus 0.85 M NaCl were subjected to Western blot analysis, and the presence of the Swf1 protein was assessed with an anti-Swf1 antibody [13]. Only clones in which a protein of the correct molecular mass was detected were pursued further, thus eliminating clones in which mutations generated premature stop codons. Strains that expressed lower but detectable levels of protein were maintained. Plasmids were purified and sequenced. When a clone contained more than one mutation, these were separated by cloning the mutated fragment of SWF1 into a plasmid containing SWF1 wt (wild-type), digested with BamHI/EcoRI, EcoRI/EcoNI or EcoNI/SalI depending on the localization of the mutation (see Supplementary Figure S1). In the case that a clone contained only one mutation, the whole mutated SWF1-coding sequence was transferred to a new 29ΔEcoRI plasmid to discard mutations in other regions of the plasmid. The resulting plasmids were re-sequenced and transformed into a *swf1Δ* strain, and the phenotypes were re-tested.

Biotinylation assays, protein electrophoresis and Western blots

PAT SDS/PAGE and Western blots were performed as previously described. Anti-Swf1 antibody was described in [13]. Anti-Tlg1 antibody was described in [25]. Biotinylation assays were performed as described in [13].

Purification of GST, wt and mutant GST–DHHC chimaeras and zinc measurements

pGEX-4T3, pJV501 and the plasmids encoding the mutated DHHC-CRDs were transformed into the *Escherichia coli* BL21(DE3) strain. Cultures were grown to a D_{600} of 0.6–0.8 at 37 °C, induced for 5 h with 0.5 mM IPTG (Promega), collected by centrifugation and frozen at − 20 °C.

In the case of GST-expressing cells, the pellet was resuspended in buffer L (20 mM Tris/HCl, pH 7.4, 250 mM NaCl, 0.5 mM $ZnSO_4$ and 2.5 mM DTT) and lysed in an C3 Emulsiflex high-pressure homogenizer (Avestin) at 15000–20000 psi (1 psi = 6.9 kPa) for 4 min, the lysate was centrifuged

© The Authors Journal compilation © 2013 Biochemical Society

for 30 min at 12000 ***g***, and the supernatant was incubated with glutathione–Sepharose 4B (GE Healthcare) for 2 h at room temperature (24 °C). The resin was extensively washed with buffer L, and then with buffer L previously incubated with Chelex 100 Resin (Bio-Rad Laboratories). Finally the protein was eluted in metal-depleted buffer E (50 mM Tris/HCl, pH 8, and 200 mM gluthathione)

In the case of cells expressing wt or mutated GST–DHHC, the pellet was resuspended in buffer A (20 mM Tris/HCl, pH 7.4, and 250 mM NaCl) and lysed in an C3 Emulsiflex high-pressure homogenizer at 15000–20000 psi for 4 min, the lysate was centrifuged for 30 min at 12000 ***g***, and the pellet was washed three times with buffer B (buffer A plus 1 % Triton X-100) to purify the inclusion bodies. The inclusion bodies were solubilized in buffer C (buffer A plus 8 M urea) for 5 h with agitation.

The protein concentration in the solubilized inclusion bodies was measured using the Bradford method (Bio-Rad Laboratories) and the protein was diluted to approximately 1 mg/ml. The protein was reduced by incubation with 100 mM DTT for 30 min at 60 °C, and dialysed against buffer L using dialysis tubing cellulose membrane 12000 Da MWCO (molecular mass cut-off) (Sigma–Aldrich). It was dialysed for 5 h against 50 volumes, and then against a further 50 volumes overnight. After dialysis, the protein solution was centrifuged for 30 min at 17000 ***g*** to remove aggregated protein. The protein that remained in the supernatant was incubated with glutathione–Sepharose 4B overnight at 4 °C. The resin was extensively washed with buffer L, and then with buffer L previously incubated with Chelex 100 Resin. Finally the proteins were eluted in metal-free buffer E.

The eluted proteins were incubated with 2 % Chelex 100 resin to remove soft bound metal, quantified by the Bradford method, and processed in triplicates for the measurement of the zinc content. Zinc was quantified by ICP-MS (inductively coupled plasma MS) at the ISIDSA facility (Facultad de Ciencias Químicas, Universidad Nacional de Córdoba, Córdoba, Argentina). The values (mol of zinc per mol of protein) obtained for the GST samples, which were typically very low, were subtracted from those of the GST–DHHC samples. The values obtained for the triplicates for each preparation were averaged and are given ± S.D.

Bioinformatics

Dataset construction

Protein sequences for *Saccharomyces cerevisiae* and *Homo sapiens* PATs were gathered from the Uniprot database (http://www.uniprot.org/). The OrthoDB database (http://cegg.unige.ch/orthodb6) was used to gather orthologous sequences from other organisms. When incomplete or low-quality sequences were found, all sequences from that organism were removed from the dataset. In the case of fungal PATs, the final dataset contains 109 protein sequences which were gathered from 19 fungal organisms. Protein sequences were aligned using a combination of MUSCLE [26] and ClustalX, and manually refined with the aid of secondary structure predictions and ClustalX and GeneDoc software. Alignment Figures were prepared using Jalview (http://www.jalview.org/).

Phylogenetics

Regions of the alignment that were deemed to be of poor quality were either removed from the alignment, or realigned only for members of an orthologue group. ML (maximum likelihood) analyses were performed using RAxML 7.2.6 in combination with the WAG amino acid replacement matrix which was determined by Prottest [27] to be the model of protein evolution which best fits the data. The best ML tree was determined with the PROTGAMMAWAG + F model with four gamma rate categories, in multiple inferences using ten randomized parsimony starting trees. Statistical support was evaluated with 1000 rapid bootstrap replicates (RAxML v7.2.8 [28] under the WAG + CAT + F approximation [29]) of rate heterogeneity, and percentage support for each bipartition among these 1000 bootstrapped trees was mapped on to the best scoring ML tree from the previous step.

Remote homology detection

HHPred (http://toolkit.tuebingen.mpg.de/hhpred) and HHSenser were used with yeast Swf1 as a query to detect similar sequences in the PDB (http://www.pdb.org/). The alignment with 2DKT was not the highest scoring, but contained the fewest gaps.

Secondary structure prediction

Secondary structure prediction was performed using a variety of programs. The program for which prediction of the 2DKT protein sequence most closely resembled the resolved structure was PROF [30]. This same program was used to predict the secondary structure of the alignment of DHHC domains for all fungal PATs.

Homology modelling

Homology modelling was performed using MODELLER 9.9 [31] on manually aligned sequences to the 2DKT PDB entry, which contains a CTCHY zinc-finger. Energy minimization and model refinement was carried out using Modrefiner [32]. Structure quality evaluation was performed using Molprobity [33]. For some models, rotamer libraries [34] were explored for exploring possible hydrogen bonds. Molecular graphics and analyses were performed with the UCSF Chimera package [35].

RESULTS

Identification of essential residues in Swf1

We carried out a screen for lack-of-function mutants in Swf1. To this end, we took advantage of two phenotypes of the *swf1Δ* strain which is unable to grow in medium with lactate as sole carbon source or in medium with a high concentration of NaCl (0.85 M). Growth in these media is an excellent predictor of Swf1-mediated palmitoylation activity, and this has been demonstrated by directly analysing the palmitoylation status of the Swf1 substrate Tlg1 [13]. Although the basis of these phenotypes is unknown, they are not due to lack of function of any single known Swf1 substrate, but most likely to a general defect in Swf1-mediated palmitoylation. A DNA fragment encoding the Swf1 ORF was generated by error-prone PCR. The fragment was co-transformed in a *swf1Δ* strain with an appropriate gapped-plasmid which was repaired *in vivo*. A total of 30000 yeast clones were plated in SC − URA medium and then replicated to YP lactate and to YPD plus 0.85 M NaCl. Replicated colonies that failed to grow in selective medium were rescued from the SC − URA plates and analysed by SDS/PAGE and Western blotting to discard mutant proteins that contain premature termination codons which in the case of Swf1 are uninformative since we already know that the last 16 amino acids of Swf1 that bear the PaCCT motif are essential for function [12]. We were finally able to confirm 21 single point mutations that led to complete loss of function, which are indicated in Table 1 and Supplementary Figure S1. Of these mutants, one corresponds to

© The Authors Journal compilation © 2013 Biochemical Society

Table 1 Loss-of-function mutations in Swf1

The majority of the mutations were isolated in the screen described in the present study. Mutations isolated in previous studies are also listed.

Amino acid	Mutation	Reference
Asp^{126}	Alanine	The present study
Cys^{136}	Tyrosine, serine	The present study
Cys^{139}	Tyrosine	The present study
Ala^{145}	Aspartic acid	The present study
Ala^{145}	Glutamic acid	[13]
Arg^{146}	Serine	The present study
Ser^{147}	Proline	The present study
Lys^{148}	Histidine	[13]
His^{149}	Leucine, arginine	The present study
Cys^{150}	Arginine	The present study
Cys^{153}	Phenylalanine	The present study
Cys^{156}	Phenylalanine	The present study
His^{162}	Glutamine	The present study
His^{163}	Leucine, arginine	The present study
Cys^{164}	Glycine	The present study
Cys^{164}	Alanine	[19]
Cys^{170}	Serine, tyrosine	The present study
Asn^{186}	Tyrosine	The present study
Met^{190}	Arginine	The present study
Arg^{196}	Glycine	The present study
Tyr^{323}	Alanine	[12]

a mutation of the cysteine residue in the DHHC motif, the mutant C164G, in agreement with what has been shown previously for Swf1 [19]. Mutation of equivalent cysteine residues has been shown to abolish both substrate acylation and autoacylation for many PATs [15,16,19,21,22,36].

We also isolated the mutant A145D, in agreement with what was observed for a similar mutation, A145E, that we previously generated by site-directed mutagenesis owing to its possible role in the determination of specificity. Amino acids His^{163} and Ser^{147} were also among the ten top specificity determination positions that we had predicted, but not tested for Swf1 [13].

The remaining 19 mutations correspond to mutations of amino acids that had not been previously mutated in Swf1. Mutation of the amino acids equivalent (same position in an alignment, see Figure 4) to Swf1 Cys^{136}, Arg^{146}, His^{149}, Cys^{139}, Cys^{150}, Cys^{153}, Cys^{156}, His^{162}, His^{163} and Cys^{170} had been produced either for Erf2 or Pfa3 [18,37], whereas mutations of Asp^{126}, Ser^{147}, Asn^{186}, Met^{190} and Arg^{190} are novel mutations for the whole PAT family.

Of particular interest are mutations N186Y, M190R and R196G that fall within TMD4, since no essential amino acids were found in the other TMDs. This suggests that TMD4, immediately downstream of the DHHC-CRD, is indeed part of this domain (see the Discussion section).

Homology modelling predicts two zinc-binding pockets in a CCHC configuration for Swf1 DHHC-CRD

In an attempt to reveal the role of essential amino acids in Swf1, we predicted the 3D structure of Swf1 DHHC-CRD by homology modelling. Remote homology searches performed using HHPred with the Swf1 DHHC domain as a query and searching the latest version of the PDB predicted the DHHC domain to be most similar to the 2DKT structure, which belongs to Pirh2, a mouse ubiquitin ligase that has been shown to promote p53 degradation in mammals. This protein contains three types of zinc fingers: a CHY zinc finger, the CTCHY-type, which is C-terminal to the CHY-type zinc finger, and a RING finger domain. HHPred aligned Swf1 to the CHY region of 2DKT, but manual alignment determined a better fit to the CTCHY-type zinc finger. Also, a PSI-BLAST search of the CTCHY-type zinc finger sequence against the SwissProt database detects a significant similarity to fungal and human PATs within three iterations with a 1×10^{-3} E-value threshold. The CTCHY structure consists of four β-hairpins in which cysteine and histidine residues, found on alternate sides of the β-sheets, co-ordinate three zinc ions in a CCHC configuration. According to the alignment, DHHC domains only posses the first cysteine of the third zinc-binding site, and it is the cysteine residue present in the DHHC motif.

The 3D model was built using MODELLER [31]. The I-Tasser server [38] provided similar results to MODELLER (not shown) and, similarly to HHPred results, 2DKT was recognized, by threading, to be the top-ranked template for homology modelling. The DHHC-CRD structure from Swf1 was refined and optimized using ModRefiner [39]. An assessment of the quality of the model was carried out using MOLPROBITY [33] and yielded similar scores to that of the 2DKT structure. The model predicts that all cysteine residues aside from Cys^{164} (the cysteine in the DHHC motif) and His^{149} and His^{163}, form a zinc-finger-type fold, co-ordinating two zinc ions in a CCHC arrangement (Figure 1A). All of the amino acids predicted to bind zinc by the model were isolated in the screen as being essential for Swf1 function. Additionally, residues predicted to be involved in zinc co-ordination display a high degree of conservation across Swf1 orthologues (see Figure 4).

The structure consists of three class 4:4 β-hairpins, each conformed by two antiparallel β-sheets stabilized by hydrogen bonds and a loop.

The gaps present in the pairwise alignment between 2DKT and PATs mainly placed additional amino acids in the loops connecting the β-hairpins, which may explain why mutations in many amino acids conforming the tight β-turns between β-sheets are critical (see Table 1 and Figure 1A), as they are able to adopt conformations which enable the tight turns needed to connect the hairpins. Moreover the A145E mutation was shown to result in an unstable protein [13].

When not occurring in turns, essential amino acids seem to correspond to positions involved in stabilizing the second hairpin, or forming bonds between hairpins two and three.

Ser^{147} seems to stabilize the turn between hairpin 1 and 2, forming stabilizing hydrogen bonds with the backbone of Leu^{158} and Ala^{160}. It should be noted that Ser^{147} was found in the screen as an essential residue.

Additionally Lys^{148} seems to form a salt bridge with Asp^{161}. In Erf2 the position corresponding to Lys^{148} is replaced with a serine residue, which could also form hydrogen bonds with Asp^{161}.

Finally, all amino acids that form the surface of the putative triple hairpin DHHC domain are polar or charged. All hydrophobic amino acids face the interior of the 3D domain, except for a highly conserved group of amino acids near the C-terminus, which form a mostly hydrophobic surface (Figure 1B) at which centre is Cys^{164}, present in the DHHC motif, which is the only cysteine residue in the region predicted not to be involved in zinc co-ordination. This surface would be in the vicinity of the membrane, since TMD4 begins at a distance of only a few amino acids.

Mutation of Swf1 residues predicted to co-ordinate zinc result in non-functional unstable proteins *in vivo*

A zinc finger is a short independently folded domain that requires zinc co-ordination to stabilize its structure (reviewed in [40]). If this is the case for Swf1 DHHC-CRD, mutations in residues expected to co-ordinate zinc should result in inactive proteins

© The Authors Journal compilation © 2013 Biochemical Society

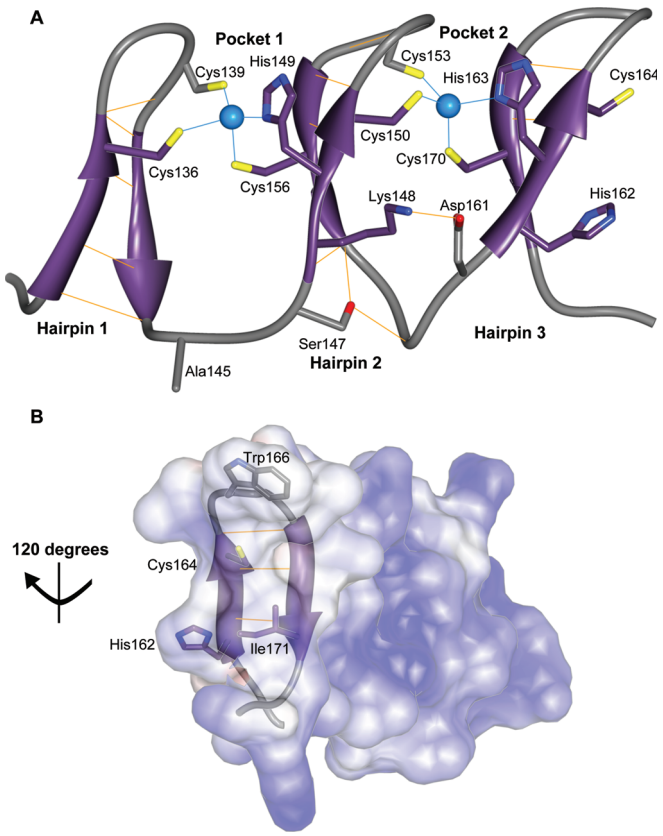

Figure 1 Ribbon diagram of the predicted 3D structure of *Saccharomyces cerevisiae* Swf1 DHHC-CRD

(**A**) Structure generated by homology modelling, using MODELLER and refined using Modrefiner, as described in the Experimental section. The model predicts two zinc-binding pockets with a CCHC configuration. β-Sheets are coloured purple, loops and carbon atoms are displayed in dark grey, sulfur atoms are yellow, oxygen atoms are red, nitrogen atoms are blue and zinc atoms are cyan. Hydrogen bonds are displayed as orange lines and metal co-ordination bonds are in cyan. (**B**) Depiction of the predicted surface for the Swf1 DHHC-CRD structure presented in (**A**), coloured according to electrostatic potential distribution. Blue denotes a positively charged surface; red denotes a negatively charged surface; white denotes neutral surfaces. For clarity, only the third hairpin of the structure in (**A**) is shown as ribbons. Highly conserved residues that form the hydrophobic surface surrounding Cys^{164} are depicted and labelled.

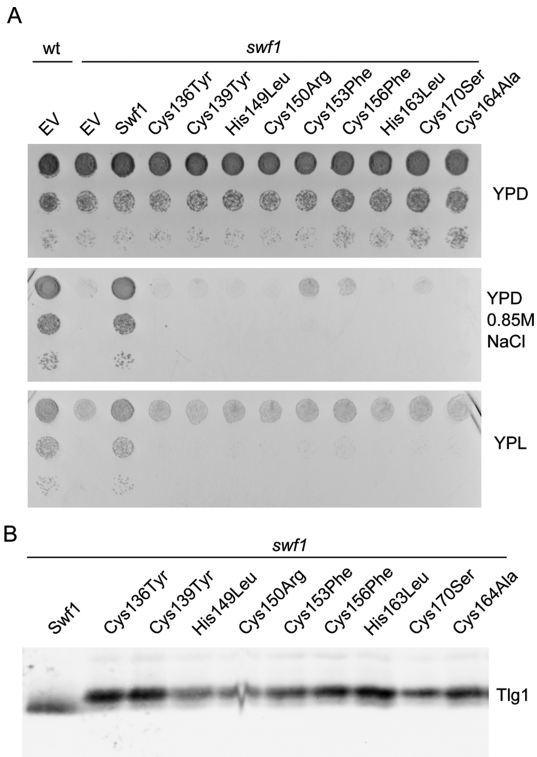

Figure 2 Mutation of residues predicted to bind zinc result in loss of function

(**A**) Serial dilution of a wt strain transformed with an empty vector (EV) or a *swf1*Δ strain transformed with empty vector or wt Swf1 and the indicated mutants, were grown on YPD, YP lactate (YPL) or YPD plus 0.85 M NaCl. (**B**) The palmitoylation status of Tlg1 was analysed in a biotinylation assay (see the Experimental section). Membrane proteins from a *swf1*Δ strain transformed with wt SWF1 or indicated mutant alleles were treated with biotin–BMCC and subjected to SDS/PAGE (12% gel) and Western blot analysis using anti-Tlg1 antibodies. Non-palmitoylated Tlg1 is modified by biotin–BMCC and shifts to higher molecular masses. Note that C164A corresponds to the cysteine residue in the DHHC motif, which is widely used as a catalytically inactive mutant for PATs.

due to lack of proper folding. Indeed, all cysteine and histidine residues from the DHHC-CRD are essential for growth in lactate or high-salt media (Figure 2A). These misfolded proteins in turn might be recognized by the cell quality control mechanism and be degraded. When we analyse the steady-state levels of these mutants by Western blotting, we observed that mutation of the residues predicted to be involved in zinc binding results in lower protein levels (Figure 3A). On the other hand, mutations C164A and H162Q, which occur in amino acids which are not predicted to bind zinc (Figure 1A), results in inactive proteins, but do not result in lower protein levels (Figure 3A). Lack of Swf1 palmitoylation activity was analysed directly by assessing the palmitoylation status of its substrate Tlg1. Since Tlg1 has only two cysteine residues and they are both palmitoylated, total protein extracts can be directly biotinylated with the *N*-ethylmalemide derivative biotin–BMCC {1-biotinamido-4-[4-(maleimidomethyl)-cyclohexane-carboxamido]butane}, and only non-palmitoylated Tlg1 will be modified, which results in a shift to higher molecular masses in SDS/PAGE. Figure 2(B) shows that endogenous Tlg1 is not palmitoylated in a *swf1*Δ strain complemented with any of the mutants putatively involved in zinc co-ordination. As a positive control, a wt SWF1 plasmid was included. Empty vector and a C164A mutant (DHHA) were included as negative controls.

To confirm that the low steady-state levels of the mutant proteins arise from misfolding and recognition by the quality control machinery, we assessed the steady-state levels of these mutants in strains defective in different degradation pathways. Pep4 is a vacuolar aspartyl protease required for the post-translational maturation of several vacuolar proteases, thus in the *pep4*Δ strain, vacuolar degradation function is severely impaired [41,42]. The levels of the wt and mutated proteins in this strain and the differences between them remain equivalent (results not shown), indicating that the degradation of the mutants does not occur through this pathway. On the other hand, deletion of the ubiquitin-conjugating enzyme Ubc7, involved in ERAD (endoplasmic reticulum-associated degradation) [43,44], does partially restore the levels of the mutant proteins (Figure 3B and Supplementary Figure S2 at http://www.biochemj.org/bj/454/bj4540427add.htm), indicating that the increased degradation of this mutant occurs through this pathway.

Swf1 DHHC-CRD is a *bona fide* zinc-binding domain

To measure directly zinc bound to Swf1, we attempted to purify Swf1 from yeast; however, this protein is highly hydrophobic and

© The Authors Journal compilation © 2013 Biochemical Society

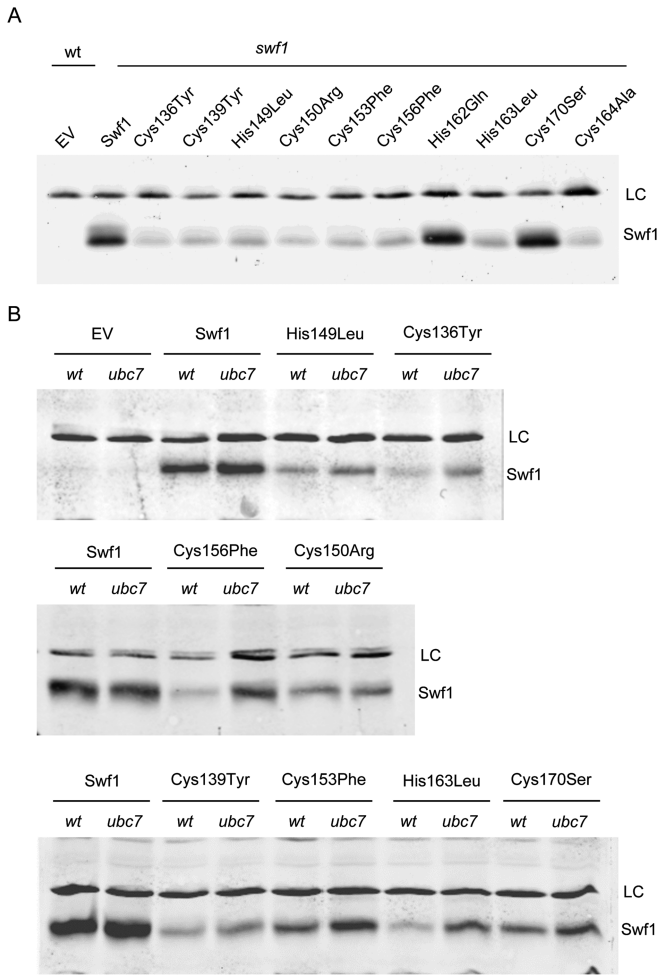

Figure 3 Mutants in residues predicted to bind zinc have reduced stability due to degradation via the ERAD pathway

(**A**) Western blot analysis of wt and mutant Swf1 in a *swf1Δ* strain. Membrane fractions were subjected to SDS/PAGE (??% gel) and Western blot analysis and developed using an anti-Swf1 antibody. A non-specific band detected by the antibody is used as loading control (LC). A wt strain transformed with an empty vector (EV) was included as a control where endogenous Swf1 is not detected under these conditions. (**B**) Western blot analysis of wt and mutant Swf1 in wt or *ubc7Δ* strains, as indicated. Membrane fractions were subjected to SDS/PAGE (12 % gel) and Western blot analysis and developed using an anti-Swf1 antibody. A non-specific band detected by the antibody is used as a loading control (LC). The Western blots shown are representative of three independent experiments for each mutant. Quantifications of these experiments are shown in Supplementary Figure S2 (at http://www.biochemj.org/bj/454/bj4540427add.htm).

very poorly expressed even under the control of strong promoters. What little is purified is unstable in solution, so we were unable to obtain measurable amounts of purified Swf1.

Instead, we decided to express and purify Swf1 DHHC-CRD from *E. coli*. To this end, we generated a GST-tagged version of the whole cytosolic loop of Swf1, comprising of the residues between TMD3 and TMD4 (from Met^{103} to Gln^{178}) and therefore containing almost the whole Swf1 DHHC-CRD (Supplementary Figure S1). We built this plasmid using wt Swf1 and mutants H162Q, C156F, C150R and H163L. The TMD4 of Swf1 is not included in our recombinant DHHC polypeptide, and, although it should be considered part of the DHHC domain, it is not predicted to be involved in zinc binding.

The fusion proteins were expressed at very high levels, but localized to inclusion bodies. This is a common feature of zinc-finger-containing proteins expressed in bacteria [45,46], possibly due to aberrant disulfide bridge formation in the bacterial cytosol. The fusion proteins were recovered from inclusion bodies by solubilization in 8 M urea, refolded by dialysis and purified by affinity chromatography. The refolded peptides were incubated with the Chelex 100 cation-exchange resin, to remove weakly bound zinc ions. The zinc content in the samples and in free GST samples purified in parallel was determined by ICP-MS. Although there was variability between different protein preparations, we consistently were able to detect zinc in levels significantly above those detected for free GST protein purified in parallel.

Table 2 Zinc content of recombinant wt and mutated Swf1 DHHC-CRDs

GST-fused wt or mutated Swfl DHHC-CRDs were expressed as inclusion bodies in *E. coli* and refolded *in vitro*, and zinc content was measured by ICP-MS. Each independent experiment was measured in triplicate. ND, not determined.

Experiment	wt	H162Q	C156F	C150R	H163L
1	1.96 ± 0.07	1.75 ± 0.08	0.98 ± 0.08	ND	ND
2	1.60 ± 0.20	1.60 ± 0.30	1.20 ± 0.20	ND	ND
3	1.41 ± 0.09	ND	ND	1.00 ± 0.40	1.10 ± 0.10
Mean	1.60	1.70	1.10	1.00	1.10

Table 2 shows the values of mol of zinc per mol of protein obtained for wt Swf1 DHHC domain and for the mutated domains. The wt protein and the mutant H162Q, which is not predicted to be involved in zinc co-ordination (Figure 1A), present zinc levels of approximately 1.7 mol of zinc per mol of protein. On the other hand, mutants C150R, C156F and H163L that would be involved in zinc co-ordination, and thus would have lost one of the zinc-binding pockets, present levels close to 1 mol of zinc per mol of protein.

Sequence analysis of DHHC domains of PATs

We next analysed the sequences of all fungal PATs present for complete genomes in OrthoMCL (109 PATs for 19 fungal organisms) for the presence of putative zinc-binding pockets. The sequences from DHHC (CRD or non-CRD) domains were aligned with the sequence of the CTCHY-zinc finger domain of Pirh2, used to generate the 3D model of the Swf1 DHHC domain. Figure 4 shows an alignment of 23 PAT orthologues from four selected fungal organisms to illustrate the results from the larger alignment.

Fungal PATs were found to have a variable number of zinc fingers, with zero, one or two for Akr1 orthologues, one or two for Pfa3 and Pfa4, zero or one for Pfa5, one or two for Swf1 and two for Erf2. The fact that the number of zinc fingers can differ even between orthologues suggests that the fold required for catalysis can be acquired without the need for two or even one zinc finger, and that, indeed, zinc itself is not involved in the catalysis mechanism. Besides, zinc atoms with four amino acid ligands usually play structural roles as opposed to catalytic site zinc atoms, which are in general co-ordinated by three amino acids and a water molecule [47,48]

Supplementary Figure S3 (at http://www.biochemj.org/bj/454/bj4540427add.htm) shows a phylogenetic analysis of DHHC domains indicating the presence or absence of the zinc-binding pockets for all fungal organisms. We did not find any Erf2 orthologues with mutations in any of the residues putatively involved in zinc binding. Akr1 orthologues from organisms belonging to the Saccharomycotina subphylum have lost both pockets (with three amino acid changes in the first pocket and four in the second), leaving only two conserved cysteine residues in the DHHC-CRD of these proteins: the one present

© The Authors Journal compilation © 2013 Biochemical Society

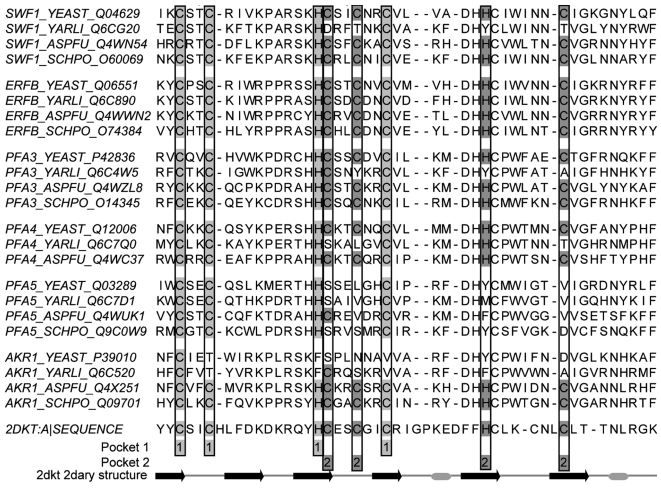

Figure 4 Conservation of residues involved in zinc co-ordination for selected fungal PATs

The regions corresponding to the DHHC domains of selected fungal PATs were aligned to the mouse Pirh2 zinc finger protein sequence whose 3D structure is available (PDB code 2DKT). Residues involved in zinc co-ordination are boxed, the corresponding residue is shaded in grey only when it is conserved. The secondary (2dary) structure of Pirh2 is displayed below; β-sheets are displayed as black arrows and α-helices as grey ovals. Notice the loss of all residues predicted to form the second zinc-binding pocket in *Y. lipolytica* Swf1.

in the DHHC motif and the first cysteine residue of the domain. Organisms that diverged earlier (belonging to the Pezizomycotina or Taphrinomycotina subphylum) display two intact zinc-binding pockets. Pfa3 orthologues also display two intact zinc-binding pockets, except for a subgroup of the Saccharomycotina subphylum in which two or three amino acids from the second pocket have changed.

Pfa4 orthologues posses two conserved zinc-binding pockets, except for the *Y. lipolytica* orthologue, which has lost the second pocket (three amino acids changed). Pfa5 orthologues have all lost the second pocket, whereas a subset of the Saccharomycotina Pfa5 orthologues have also lost the first pocket.

More importantly, whenever a residue predicted to form a zinc-binding pocket is mutated, other residues predicted to be involved in the formation of that particular pocket are lost (see Figure 4). This indicates that the selective pressure to keep these residues disappears upon the loss of one of them and suggests a common function that requires all four residues. This observation further supports the structural prediction of zinc co-ordination by PATs.

We extended our analyses to mammalian PATs. All mammalian PATs are predicted to have two CCHC-type zinc fingers, with the exception of DHHC22, which has lost two residues of the second pocket (results not shown and mentioned in [21]).

Non-cysteine-rich DHHC domains may adopt a similar structure to DHHC-CRDs

The sequence analysis indicates that, in the case of Swf1, all of its orthologues possess two conserved zinc-binding pockets, except for the *Y. lipolytica* Swf1 orthologue, which has lost the second pocket, with mutations appearing in all four amino acids that compose the second pocket (Figure 4). There are several examples of metal-binding protein relatives that have lost their zinc-binding residues, but still retain a highly similar fold; zinc co-ordination could be replaced by different structure-stabilizing elements [49]. If this is the case for Swf1, we speculated that the *Y. lipolytica* Swf1 protein should function in yeast. Indeed,

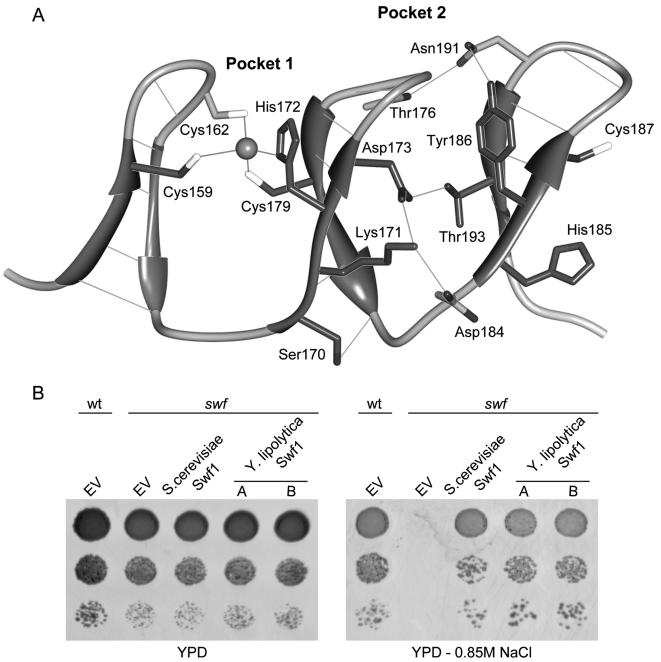

Figure 5 *Y. lipolytica* Swf1 complements a *S. cerevisiae swf1Δ* strain despite the absence of one zinc-binding pocket

(**A**) Ribbon diagram of the predicted 3D structure of *Y. lipolytica* Swf1 DHHC-CRD. The model predicts one zinc-binding pocket with a CCHC configuration. Residues that form novel hydrogen bonds between the second and third hairpin replace the residues that co-ordinate zinc in the second zinc-binding pocket of *S. cerevisiae* Swf1. Hydrogen bonds and metal co-ordination bonds are shown as thin lines. (**B**) Complementation of *S. cerevisiae swf1Δ* strain with *Y. lipolytica* SWF1 orthologue. Serial dilutions of a wt or *swf1Δ* strain transformed with an empty vector (EV) and with either *S. cerevisiae* Swf1 or *Y. lipolytica* Swf1 (A and B are two independent transformants) were grown in YPD, YPD plus high salt and YP lactate. Both *S. cerevisiae* Swf1 and *Y. lipolytica* Swf1 are expressed from CEN plasmids and driven by the TPI1 promoter.

expression of *Y. lipolytica* Swf1 in a *Δswf1* strain suppresses the phenotypes (lack of growth in lactate and high salt) of the gene deletion (Figure 5B), reinforcing the idea that the fold required for PAT activity can be attained by alternative mechanisms that do not require zinc co-ordination.

We next modelled the DHHC domain of *Y. lipolytica* Swf1 using yeast Swf1 as a template. Figure 5(A) shows the *Y. lipolytica* Swf1 3D model that possesses one zinc-binding pocket and a very similar second pocket which does not contain zinc; instead, the structure is stabilized by hydrogen bonds. The replacement of the cysteine residues by aspartic acid and the threonine and histidine residues by tyrosine supports this model, since these are residues that have a good capacity to form hydrogen bonds. Overall, the whole domain is very similar to that of yeast Swf1, which explains the complementation assays. This phenomenon may be also valid for other non-CRD PATs, since visual inspection of the residues that replace the cysteine and histidine residues show a pre-eminence of residues that are prone to form hydrogen bonds (see Figure 4).

DISCUSSION

Although there has been progress in identifying palmitoylated substrates and their PATs, particularly in yeast, less is known about PATs themselves. We have carried out a screen to uncover new lack-of-function mutations in Swf1 and obtained several mutations, which map to the DHHC-CRD. The fact that no mutations were isolated outside the DHHC-CRD is intriguing.

© The Authors Journal compilation © 2013 Biochemical Society

Regions outside the DHHC domain are poorly conserved, even among orthologues from closely related organisms [12]. Yet chimaeric protein analyses indicate that regions outside the DHHC domain are also required for function and cannot be replaced by that of other PATs (A. González Montoro and J. Valdez Taubas, unpublished work). It is possible that we have missed mutations outside the DHHC-CRD because of the way the screen was carried out. The use of overexpressed proteins only allows the detection of mutations with extreme phenotypes.

Several conclusions can be drawn from the mutational analysis of Swf1; three mutations are embedded within the region corresponding to the TMD that follows the DHHC domain (TMD4). We have often wondered whether this TMD should be included as part of the DHHC domain. Conservation analysis within this region is complicated by the requirement of residues to be hydrophobic. The isolation of mutants in this region, compared with none in the other TMDs, suggests that this TMD is critical for activity and can indeed be considered part of the DHHC domain as initially suggested [23].

In the present study we show, for the first time, that a DHHC-CDR is indeed able to bind zinc. Using homology modelling of Swf1 DHHC-CRD, we postulate that residues Cys^{136}, Cys^{139}, His^{149}, Cys^{150}, Cys^{153}, Cys^{156}, His^{163} and Cys^{170} are involved in zinc co-ordination. Remarkably, all of these residues were found in the screen as amino acids that result in lack of function when mutated. It appears that loss of any of these residues results in a catastrophic loss of structure, which leads to protein degradation and loss of function. We speculate that the loss of function is not solely due to protein degradation, because the proteins, although degraded, are still present at higher levels than endogenous Swf1 (Figure 3A), indicating that the structure provided by the zinc fingers is required for function.

All amino acids predicted to be involved in zinc co-ordination are conserved in Erf2, and were mutated by Mitchell et al. [21]. Replacement of Cys^{209} by a serine residue produced an intermediate phenotype, and mutation of the other seven residues resulted in an inactive protein. Mutation of all of these amino acids produced a less stable protein [21], in agreement with the structural role we propose for the zinc finger.

The structural model of the DHHC-CRD of Swf1 suggests that it is a novel structure which is similar to the CTCHY domain, represented by 2DKT in the PDB database, and that does not fit into any of the existing structural classifications of zinc fingers [50,51]. The model is neatly supported by the mutational data, not only at the level of zinc co-ordination, but also by mutations in residues that are predicted to form salt bridges that stabilize the structure.

It has been postulated that the palmitoylation reaction occurs through a palmitoyl–PAT intermediate in the cysteine residue of the DHHC motif (Cys^{164} for Swf1). This intermediate can be hydrolysed in the absence of substrate [21]. The conserved hydrophobic surface at the C-terminus of the DHHC domain may play a crucial role in restricting water accessibility to the active site, thus allowing for higher palmitoyl–PAT intermediate levels.

Zinc binding by PATs has been assumed, but it had not been demonstrated. In the present study we show that a DHHC-CRD is indeed able to bind zinc and provide an indication of how this co-ordination may be attained for Swf1 and possibly for other PATs. Our zinc measurements are in good agreement with the model proposed for Swf1 DHHC-CRD, since the values obtained for wt and H162Q mutant are close to 1.7 moles of zinc per mole of protein and the values for mutants in amino acids predicted to be involved in zinc co-ordination (C156F, C150R and H163L) are close to 1. The difference between the values we measure for wt DHHC-CRD and the expected value of 2 mol of zinc of per mol of protein may be due to incomplete or aberrant refolding of the DHHC-CRD. We believe that these measurements, together with the mutational analyses and mutant protein stability data, support the proposed model of zinc co-ordination by Swf1 DHHC-CRD.

Since the DHHC domain is probably the catalytic domain of PATs, why some are cysteine-rich and others are not was intriguing. The complementation of yeast *swf1Δ* strain by *Y. lipolytica* Swf1, which lacks one zinc-binding pocket, and the modelling of the 3D structure of its DHHC domain suggest that both CRD and non-CRD PATs would probably have very similar structures and therefore similar mechanisms for protein palmitoylation. Overall, the results shown in the present study, which assign a role to many of the residues within the DHHC motifs, may aid in the understanding of the structure–function relationships of PATs and ultimately the mechanism of protein palmitoylation.

AUTHOR CONTRIBUTION

Ayelén González Montoro and Javier Valdez Taubas designed the experiments. Ayelén González Montoro conducted the experiments. Rodrigo Quiroga performed the bioinformatic analyses. Javier Valdez Taubas supervised the whole project. Ayelén González Montoro, Rodrigo Quiroga and Javier Valdez Taubas analysed and interpreted the results and contributed to writing and revising the paper.

ACKNOWLEDGEMENTS

We thank Dr José L. Barra and Dr Hugo Maccioni for critically reading the paper prior to submission, and Dr Mario Ermácora for kindly supplying a strain of *Yarrowia lipolytica*.

FUNDING

This work was supported by the Secretaría de Ciencia y Tecnología, Universidad Nacional de Córdoba and Agencia Nacional de Promoción Científica y Tecnológica, Argentina [grant number PICT 1102 (to J.V.T.)]. A.G.M. and R.Q. are recipients of fellowships from CONICET (Consejo Nacional de Ciencia y Tecnología de Argentina). J.V.T. is a Career Investigator of CONICET (Argentina).

REFERENCES

1 Berthiaume, L. and Resh, M. D. (1995) Biochemical characterization of a palmitoyl acyltransferase activity that palmitoylates myristoylated proteins. J. Biol. Chem. **270**, 22399–22405
2 Bijlmakers, M. J. and Marsh, M. (2003) The on-off story of protein palmitoylation. Trends Cell Biol. **13**, 32–42
3 DeMar, Jr, J. C. and Anderson, R. E. (1997) Identification and quantitation of the fatty acids composing the CoA ester pool of bovine retina, heart, and liver. J. Biol. Chem. **272**, 31362–31368
4 Kang, R., Wan, J., Arstikaitis, P., Takahashi, H., Huang, K., Bailey, A. O., Thompson, J. X., Roth, A. F., Drisdel, R. C., Mastro, R. et al. (2008) Neural palmitoyl-proteomics reveals dynamic synaptic palmitoylation. Nature **456**, 904–909
5 Smotrys, J. E., Schoenfish, M. J., Stutz, M. A. and Linder, M. E. (2005) The vacuolar DHHC-CRD protein Pfa3p is a protein acyltransferase for Vac8p. J. Cell Biol. **170**, 1091–1099
6 Washbourne, P. (2004) Greasing transmission: palmitoylation at the synapse. Neuron **44**, 901–902
7 Xue, L., Gollapalli, D. R., Maiti, P., Jahng, W. J. and Rando, R. R. (2004) A palmitoylation switch mechanism in the regulation of the visual cycle. Cell **117**, 761–771
8 Korycka, J., Lach, A., Heger, E., Boguslawska, D. M., Wolny, M., Toporkiewicz, M., Augoff, K., Korzeniewski, J. and Sikorski, A. F. (2012) Human DHHC proteins: a spotlight on the hidden player of palmitoylation. Eur. J. Cell Biol. **91**, 107–117
9 Linder, M. E. and Deschenes, R. J. (2007) Palmitoylation: policing protein stability and traffic. Nat. Rev. Mol. Cell Biol. **8**, 74–84

© The Authors Journal compilation © 2013 Biochemical Society

10 Lakkaraju, A. K., Abrami, L., Lemmin, T., Blaskovic, S., Kunz, B., Kihara, A., Dal Peraro, M. and van der Goot, F. G. (2012) Palmitoylated calnexin is a key component of the ribosome-translocon complex. EMBO J. **31**, 1823–1835
11 Lu, D., Sun, H. Q., Wang, H., Barylko, B., Fukata, Y., Fukata, M., Albanesi, J. P. and Yin, H. L. (2012) Phosphatidylinositol 4-kinase IIα is palmitoylated by Golgi-localized palmitoyltransferases in cholesterol-dependent manner. J. Biol. Chem. **287**, 21856–21865
12 Gonzalez Montoro, A., Quiroga, R., Maccioni, H. J. and Valdez Taubas, J. (2009) A novel motif at the C-terminus of palmitoyltransferases is essential for Swf1 and Pfa3 function *in vivo*. Biochem. J. **419**, 301–308
13 Gonzalez Montoro, A., Chumpen Ramirez, S., Quiroga, R. and Valdez Taubas, J. (2011) Specificity of transmembrane protein palmitoylation in yeast. PLoS ONE **6**, e16969
14 Mitchell, D. A., Vasudevan, A., Linder, M. E. and Deschenes, R. J. (2006) Protein palmitoylation by a family of DHHC protein S-acyltransferases. J. Lipid Res. **47**, 1118–1127
15 Lam, K. K., Davey, M., Sun, B., Roth, A. F., Davis, N. G. and Conibear, E. (2006) Palmitoylation by the DHHC protein Pfa4 regulates the ER exit of Chs3. J. Cell Biol. **174**, 19–25
16 Lobo, S., Greentree, W. K., Linder, M. E. and Deschenes, R. J. (2002) Identification of a Ras palmitoyltransferase in *Saccharomyces cerevisiae*. J. Biol. Chem. **277**, 41268–41273
17 Roth, A. F., Wan, J., Bailey, A. O., Sun, B., Kuchar, J. A., Green, W. N., Phinney, B. S., Yates, 3rd, J. R. and Davis, N. G. (2006) Global analysis of protein palmitoylation in yeast. Cell **125**, 1003–1013
18 Hou, H., John Peter, A. T., Meiringer, C., Subramanian, K. and Ungermann, C. (2009) Analysis of DHHC acyltransferases implies overlapping substrate specificity and a two-step reaction mechanism. Traffic **10**, 1061–1073
19 Valdez-Taubas, J. and Pelham, H. (2005) Swf1-dependent palmitoylation of the SNARE Tlg1 prevents its ubiquitination and degradation. EMBO J. **24**, 2524–2532
20 Mill, P., Lee, A. W., Fukata, Y., Tsutsumi, R., Fukata, M., Keighren, M., Porter, R. M., McKie, L., Smyth, I. and Jackson, I. J. (2009) Palmitoylation regulates epidermal homeostasis and hair follicle differentiation. PLoS Genet. **5**, e1000748
21 Mitchell, D. A., Mitchell, G., Ling, Y., Budde, C. and Deschenes, R. J. (2010) Mutational analysis of *Saccharomyces cerevisiae* Erf2 reveals a two-step reaction mechanism for protein palmitoylation by DHHC enzymes. J. Biol. Chem. **285**, 38104–38114
22 Jennings, B. C. and Linder, M. E. (2012) DHHC protein S-acyltransferases use similar ping-pong kinetic mechanisms but display different acyl-CoA specificities. J. Biol. Chem. **287**, 7236–7245
23 Putilina, T., Wong, P. and Gentleman, S. (1999) The DHHC domain: a new highly conserved cysteine-rich motif. Mol. Cell. Biochem. **195**, 219–226
24 Bohm, S., Frishman, D. and Mewes, H. W. (1997) Variations of the C2H2 zinc finger motif in the yeast genome and classification of yeast zinc finger proteins. Nucleic Acids Res. **25**, 2464–2469
25 Holthuis, J. C. M., Nichols, B. J. and Pelham, H. R. B. (1998) The syntaxin Tlg1p mediates trafficking of chitin synthase III to polarized growth sites in yeast. Mol. Biol. Cell **9**, 3383–3397
26 Edgar, R. C. (2004) MUSCLE: multiple sequence alignment with high accuracy and high throughput. Nucleic Acids Res. **32**, 1792–1797
27 Abascal, F., Zardoya, R. and Posada, D. (2005) ProtTest: selection of best-fit models of protein evolution. Bioinformatics **21**, 2104–2105
28 Stamatakis, A., Hoover, P. and Rougemont, J. (2008) A rapid bootstrap algorithm for the RAxML Web servers. Syst. Biol. **57**, 758–771
29 Stamatakis, A. (2006) Phylogenetic models of rate heterogeneity: a high performance computing perspective. 20th IEEE International Parallel & Distributed Processing Symposium, Rhodes Island, Greece, 25–29 April 2006, Abstract 278
30 Rost, B. (2001) Review: protein secondary structure prediction continues to rise. J. Struct. Biol. **134**, 204–218
31 Eswar, N., Webb, B., Marti-Renom, M. A., Madhusudhan, M. S., Eramian, D., Shen, M. Y., Pieper, U. and Sali, A. (2006) Comparative protein structure modeling using Modeller. Curr. Protoc. Bioinf. **15**, 5.6.1–5.6.30
32 Ramachandran, S., Kota, P., Ding, F. and Dokholyan, N. V. (2011) Automated minimization of steric clashes in protein structures. Proteins **79**, 261–270
33 Chen, V. B., Arendall, 3rd, W. B., Headd, J. J., Keedy, D. A., Immormino, R. M., Kapral, G. J., Murray, L. W., Richardson, J. S. and Richardson, D. C. (2010) MolProbity: all-atom structure validation for macromolecular crystallography. Acta Crystallogr., Sect. D: Biol. Crystallogr. **66**, 12–21
34 Dunbrack, Jr, R. L. (2002) Rotamer libraries in the 21st century. Curr. Opin. Struct. Biol. **12**, 431–440
35 Pettersen, E. F., Goddard, T. D., Huang, C. C., Couch, G. S., Greenblatt, D. M., Meng, E. C. and Ferrin, T. E. (2004) UCSF Chimera – a visualization system for exploratory research and analysis. J. Comput. Chem. **25**, 1605–1612
36 Roth, A. F., Feng, Y., Chen, L. and Davis, N. G. (2002) The yeast DHHC cysteine-rich domain protein Akr1p is a palmitoyl transferase. J. Cell Biol. **159**, 23–28
37 Mitchell, D. A., Mitchell, G., Ling, Y., Budde, C. and Deschenes, R. J. (2010) Mutational analysis of *Saccharomyces cerevisiae* Erf2 reveals a two-step reaction mechanism for protein palmitoylation by DHHC enzymes. J. Biol. Chem. **285**, 38104–38114
38 Roy, A., Kucukural, A. and Zhang, Y. (2010) I-TASSER: a unified platform for automated protein structure and function prediction. Nat. Protoc. **5**, 725–738
39 Xu, D. and Zhang, Y. (2011) Improving the physical realism and structural accuracy of protein models by a two-step atomic-level energy minimization. Biophys. J. **101**, 2525–2534
40 Laity, J. H., Lee, B. M. and Wright, P. E. (2001) Zinc finger proteins: new insights into structural and functional diversity. Curr. Opin. Struct. Biol. **11**, 39–46
41 Woolford, C. A., Daniels, L. B., Park, F. J., Jones, E. W., Van Arsdell, J. N. and Innis, M. A. (1986) The PEP4 gene encodes an aspartyl protease implicated in the posttranslational regulation of *Saccharomyces cerevisiae* vacuolar hydrolases. Mol. Cell. Biol. **6**, 2500–2510
42 Ammerer, G., Hunter, C. P., Rothman, J. H., Saari, G. C., Valls, L. A. and Stevens, T. H. (1986) PEP4 gene of *Saccharomyces cerevisiae* encodes proteinase A, a vacuolar enzyme required for processing of vacuolar precursors. Mol. Cell. Biol. **6**, 2490–2499
43 Biederer, T., Volkwein, C. and Sommer, T. (1997) Role of Cue1p in ubiquitination and degradation at the ER surface. Science **278**, 1806–1809
44 Hiller, M. M., Finger, A., Schweiger, M. and Wolf, D. H. (1996) ER degradation of a misfolded luminal protein by the cytosolic ubiquitin-proteasome pathway. Science **273**, 1725–1728
45 Lee, M. S., Gippert, G. P., Soman, K. V., Case, D. A. and Wright, P. E. (1989) Three-dimensional solution structure of a single zinc finger DNA-binding domain. Science **245**, 635–637
46 Nurmemmedov, E. and Thunnissen, M. (2006) Expression, purification, and characterization of the 4 zinc finger region of human tumor suppressor WT1. Protein Expression Purif. **46**, 379–389
47 McCall, K. A., Huang, C. and Fierke, C. A. (2000) Function and mechanism of zinc metalloenzymes. J. Nutr. **130**, 1437S–1446S
48 Vallee, B. L. and Auld, D. S. (1990) Zinc coordination, function, and structure of zinc enzymes and other proteins. Biochemistry **29**, 5647–5659
49 Torrance, J. W., Macarthur, M. W. and Thornton, J. M. (2008) Evolution of binding sites for zinc and calcium ions playing structural roles. Proteins **71**, 813–830
50 Gamsjaeger, R., Liew, C. K., Loughlin, F. E., Crossley, M. and Mackay, J. P. (2007) Sticky fingers: zinc-fingers as protein-recognition motifs. Trends Biochem. Sci. **32**, 63–70
51 Krishna, S. S., Majumdar, I. and Grishin, N. V. (2003) Structural classification of zinc fingers: survey and summary. Nucleic Acids Res. **31**, 532–550

Received 9 November 2012/15 June 2013; accepted 24 June 2013
Published as BJ Immediate Publication 24 June 2013, doi:10.1042/BJ20121693

© The Authors Journal compilation © 2013 Biochemical Society

Biochem. J. (2013) **454**, 427–435 (Printed in Great Britain) doi:10.1042/BJ20121693

online data

SUPPLEMENTARY ONLINE DATA

Zinc co-ordination by the DHHC cysteine-rich domain of the palmitoyltransferase Swf1

Ayelén GONZÁLEZ MONTORO*, Rodrigo QUIROGA* and Javier VALDEZ TAUBAS*[1]

*Centro de Investigaciones en Química Biológica de Córdoba, CIQUIBIC (UNC-CONICET), Departamento de Química Biológica, Facultad de Ciencias Químicas, Universidad Nacional de Córdoba, Ciudad Universitaria, X5000HUA Córdoba, Argentina

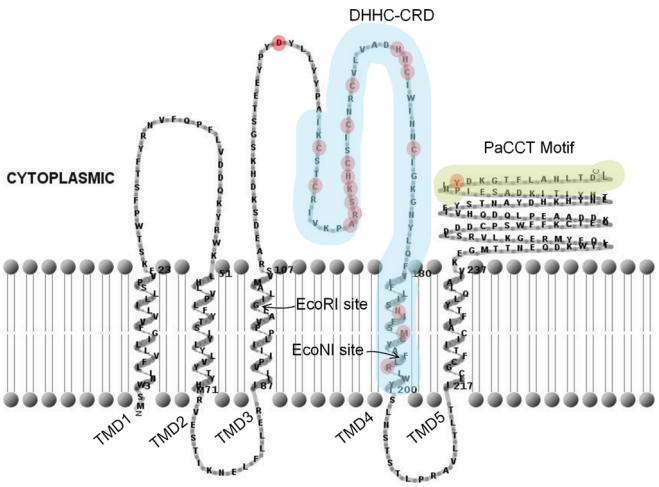

Figure S1 Schematic diagram of Swf1

The diagram shows the predicted topology of Swf1. The DHHC-CRD is highlighted in cyan and the PaCCT domain is in green. Residues that were found to result in loss of function when mutated are highlighted in red.

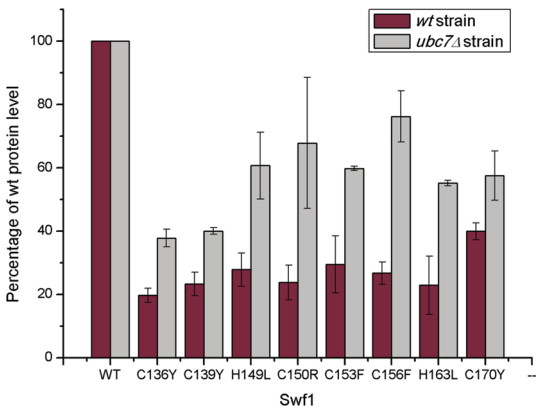

Figure S2 Quantification of steady-state levels of wt or mutant versions of Swf1 in wt and *ubc7Δ* strains

Membrane fractions of wt or *ubc7Δ* strains transformed with vectors expressing wt Swf1 or the indicated mutants were subjected to SDS/PAGE and Western blot analysis as shown in Figure 3 of the main text and developed using the anti-Swf1 antibody. The bands were quantified and normalized with the non-specific band recognized by the antibody that is used as a loading control. Results are expressed as a percentage of the wt protein. For each mutant, the values are the mean ± S.E.M. of three independent experiments.

[1] To whom correspondence should be addressed (email jvaldezt@dqb.fcq.unc.edu.ar).

© The Authors Journal compilation © 2013 Biochemical Society

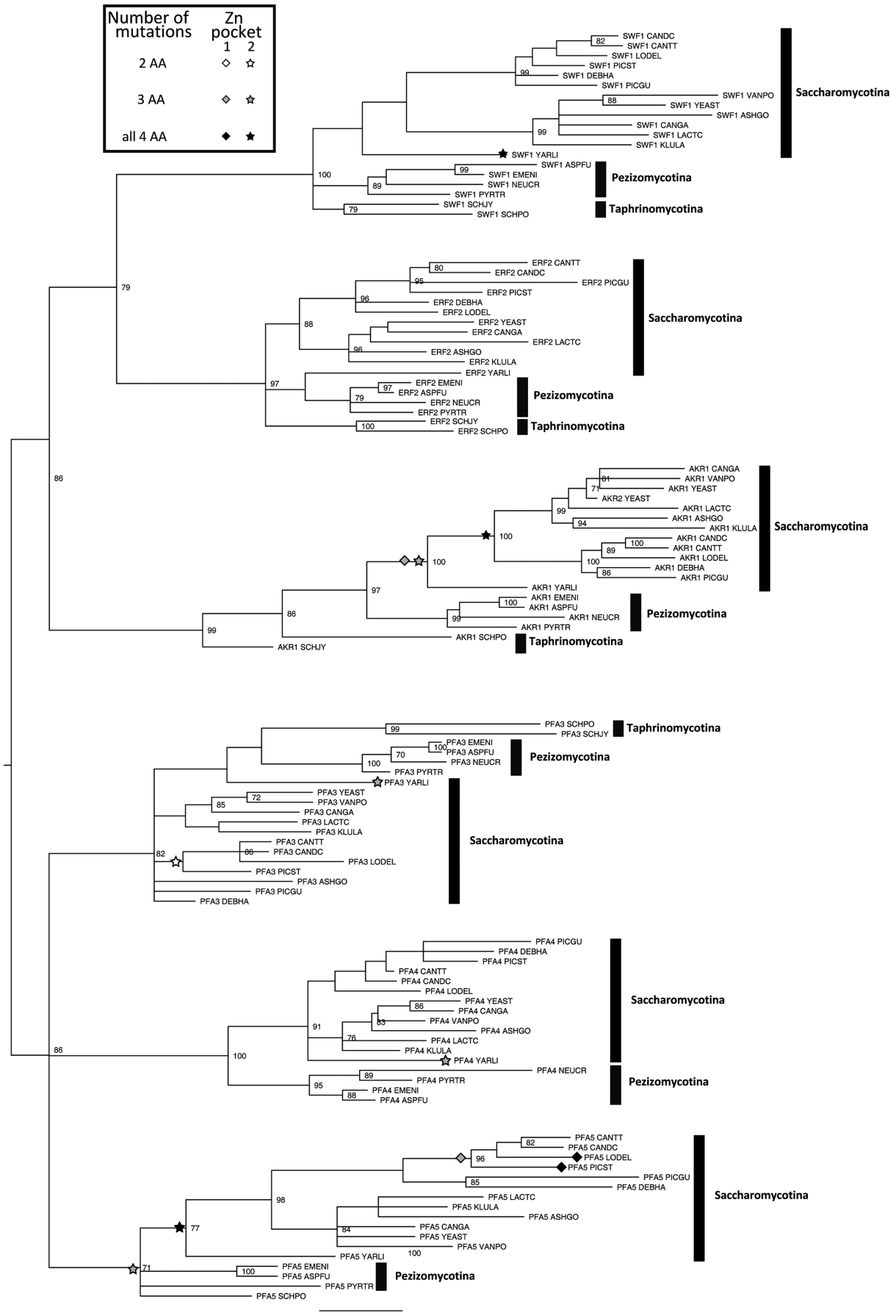

© The Authors Journal compilation © 2013 Biochemical Society

Figure S3 ML phylogenetic tree of fungal PATs displaying the occurrence of events of zinc co-ordination pocket loss

Loss of the first pocket is represented with diamonds, and loss of the second with a star. White indicates that two amino acids (of the four which co-ordinate the zinc atom) change, grey indicates that three amino acids change, and black indicates that all four amino acids change. Numbers on nodes represent percentage support for each bipartition among 100 bootstrapped trees. Nodes with less than 50 % support were removed, and support is only displayed when above 70 %.

Received 9 November 2012/15 June 2013; accepted 24 June 2013
Published as BJ Immediate Publication 24 June 2013, doi:10.1042/BJ20121693

© The Authors Journal compilation © 2013 Biochemical Society